Copper oxide nanoparticles suppress retinal angiogenesis via inducing endothelial cell cuproptosis

Haorui Zhang
Changhai Hospital
Chang Cai
Shanghai Changzheng Hospital
Qing Li
Changhai Hospital
Zheng Nie
Changhai Hospital
Mengzhu Wang
Changhai Hospital
Yongxuan Liu
Changhai Hospital
Wei Shen
Changhai Hospital
Hongyuan Song (hongyuansong@hotmail.com)
Changhai Hospital

Research Article

Keywords: Angiogenesis, Copper oxide nanoparticles, Cuproptosis, Metabolism, TCA cycle

Posted Date: September 29th, 2023

DOI: https://doi.org/10.21203/rs.3.rs-3377136/v1

Abstract

Background: Copper oxide nanoparticles (CuO NPs) have demonstrated versatile applications in antitumor and antibacterial contexts, however, their potential as an anti- angiogenesis agent remains unexplored. This study aims to comprehensively investigate the efficacy of CuO NPs in the treatment of pathological angiogenic retinopathy.

Results

We demonstrated that CuO NPs possess nano-sized dimensions and exhibit well biocompatibility. *In vitro* experiments revealed that CuO NPs impede the proliferation, tube formation, migration, and sprouting of HUVECs dose-dependently. Subsequently, *in vivo* findings showed that CuO NPs effectively suppressed the development of retinal vasculature in a mouse model, as well as alleviate pathological retinal angiogenesis in an oxygen-induced retinopathy (OIR) model. Furthermore, RNA-seq and metabolomic analysis revealed that CuO NPs disrupt the tricarboxylic acid (TCA) cycle and induce cuproptosis. These results were further supported by the evaluation of metabolites and the expression of cuproptosis-related proteins.

Conclusions

The CuO NPs exhibit potential as effective anti-angiogenic platforms for the treatment of pathological retinal angiogenesis.

1 Introduction

Pathological retinal angiogenesis is one of the vision-threatening complications of ocular vascular diseases, including retinopathy of prematurity (ROP), proliferative diabetic retinopathy (PDR), central retinal vein occlusion (RVO) and age-related macular degeneration (AMD)[1, 2]. Pan retinal photocoagulation and intraocular injection of humanized monoclonal antibodies against vascular endothelial growth factor (anti-VEGF), such as ranibizumab and aflibercept, have being used for retinal angiogenesis[3, 4]. However, many patients suffer from adverse effects of current treatments such as persistent plasma fluid exudation, unresolved or new hemorrhage and suboptimal vision recovery [5, 6]. Therefore, novel therapeutic approaches for pathological retinal angiogenesis are urgently demanded.

Copper oxide nanoparticles (CuO NPs) are extensively utilized metal oxide metal oxide nanoparticles due to their excellent physical–chemical characteristics [7]. Copper oxide nanostructures possess diverse applications in the field of biomedicine, demonstrating anticancer[8–11], antibacterial properties [12, 13] and other biomedical applications [14, 15]. Nevertheless, the role of CuO NPs to the process of pathological angiogenesis remains unclear. Cuproptosis, a novel form form of regulated cell death, is characterized by its dependence on copper and its nonapoptotic properties, its occurrence is distinct from all other established mechanisms governing cell death, including apoptosis, pyroptosis, ferroptosis, and necroptosis [16]. Research has demonstrated that cuproptosis is mainly associated with accumulation of

intracellular copper. The excessive presence of Cu^{2+} within cells is transported to the mitochondria through ionophores [17]. Within the mitochondria, Cu^{2+} interacts with mitochondrial matrix reductase ferredoxin 1 (FDX1) and undergoes reduction to Cu^{+} [16, 18]. The increased levels of Cu^{+} directly bind to lipoylated components within the tricarboxylic acid (TCA) cycle, resulting in the aggregation of lipoylated proteins and subsequent depletion of iron-sulfur cluster proteins. This sequence of events triggers proteotoxic stress and ultimately leads to cellular demise [16, 19].

In the current investigation, it was observed that CuO NPs possess the ability to impede angiogenesis both *in vitro* and *in vivo*. Additionally, the targeted metabolomics findings indicate a significant inhibition of the TCA cycle by CuO NPs, leading to an elevation in intracellular levels of pyruvate acid and alpha-ketoglutaric acid. Moreover, the transcriptomic analysis results demonstrate that CuO NPs disrupt the TCA cycle and reduce the intracellular protein expression of ferredoxin 1 (FDX1), dihydrolipoamide S-acetyltransferase (DLAT), and succinate dehydrogenase complex iron sulfur subunit B (SDHB) (Fig. 1). These outcomes were further confirmed through western blotting. The results of these experiments provide evidence that CuO NPs have the ability to induce endothelial cell (EC) cuproptosis by disrupting the TCA cycle. The data suggested that CuO NPs may hold promise as a novel anti-angiogenic drug for the treatment of pathological retinal angiogenesis.

2 Materials and methods

Materials

CuO NPs was purchased from Nanjing XFNANO Materials Tech Co., Ltd. (XF130, Nanjing, China); Cell Counting Kit- 8(CCK-8) was purchased from Dojindo Laboratories, (Dojindo, Japan); Calcein-AM/PI Live Cell/Dead Cell Double Staining Kit was obtained from Solarbio (Beijing, China). Tublin, 4',6-diamidino-2-phenylindole (DAPI) were obtained from Thermo Fisher Scientific (Shanghai, China). Cell-LightTM EdU Apollo567 Kit was purchased from Ribobio (Guangzhou, China); FITC-conjugated Isolectin B4 (IB4), Methyl cellulose and Triton-X-100 were purchased from Sigma-Aldrich (Shanghai, China). Matrigel Matrix was obtained from BD Biosciences (Shanghai, China); Antibodies to FDX1, DLAT, SDHB and β-Actin were obtained from Proteintech Group (Wuhan, China); The Pyruvate assay kit was acquired from Nanjing Jiancheng Bioengineering Institute in Nanjing, China. Additionally, all cell culture plates and dishes were obtained from Corning Life Sciences.

Cell culture

Human umbilical vein endothelial cell lines (HUVEC) were purchased from ScienCell (SanDiego, USA) and cultured in ndothelial Cell Medium (ECM, Cell Research, Shanghai, China) supplemented with 5% fetal bovine serum (FBS), 1% penicillin/streptomycin and 1% endothelial cells growth supplement (ECGS). The cells were maintained at 37°C in humidified 5% CO2, and the medium was changed every 2 days. HUVEC cells tested negative for mycoplasma.

Cell Proliferation

Cell proliferation rate was measured using EdU assays. Briefly, HUVECs were cultured in 96-well plates overnight and allowed to grow for 24 hours in the presence of CuO NPs. Subsequently, the culture medium was replaced with 100 uL of fresh medium containing EdU. Following a two-hour incubation period, the cells were fixed with 4% paraformaldehyde for 30 minutes, washed with glycine for 5 minutes and twice with 100uL 0.5% Trion X-100. They were then stained with 100uL of Apollo Dye Solution in darkness for 30 minutes, rinsed three times with 100 μL of 0.5% Trion X-100, and subsequently dyed with Hoechst for 30 minutes. The cells were subsequently rinsed thrice with PBS, followed by acquisition of images using a fluorescence microscope (IX81, Olympus). Statistical analysis was conducted using the ImageJ software.

Cell Migration

Cell migration was assessed utilizing a wound healing technique. Briefly, a total of 1×105 cells were seeded in a 2-well ibidi chamber plate to establish a confluent monolayer. Subsequently, the cells were subjected to a 24-hour pretreatment with CuO NPs. Following this, the insert was lifted, and the cells were washed thrice with PBS to eliminate any suspended cells, after which they were cultured with the initial medium. Microscopic images were captured at 0 hours and 16 hours using an Olympus IX81 microscope. All images were processed using ImageJ software.

Tube Formation

The Matrigel tube formation assay was conducted to evaluate the impact of CuO NPs on angiogenesis. Initially, 100 μL of Matrigel (12 mg/mL) was dispensed onto a pre-cooled 96-well plate and allowed to solidify at 37°C for a duration of 1.5 hours. Subsequently, HUVECs that had been exposed to either a control or CUO-NPs for a period of 24 hours were enzymatically detached using trypsin, and 1×10^4 cells were seeded into the aforementioned 96-well plate. Following an incubation period of 2 hours at 37°C, microscopic images were captured using an Olympus IX81 microscope, and the tube length was determined utilizing ImageJ software.

Sprouting Assay

Spheroid sprouting assay was conducted to evaluate the effects of CuO NPs on angiogenesis

in vitro. Initially, HUVECs were trypsinized and resuspended into control medium or medium containing CuO NPs at a density of 2×10^4 cells/mL. The cells were combined with 1 mL of methocel stock solution and subsequently transferred to a sterile multichannel pipette reservoir. A volume of 25 μL of the solution was then dispensed onto a 10 cm square petri dish using a pipette. Subsequently, the dish was inverted and placed in a cell culture incubator for a duration of 24 hours. The resulting spheroids were delicately rinsed with 10 mL of PBS and subsequently transferred into a 15 mL conical tube. The spheroids were subjected to centrifugation at a force of 200 g for a duration of 5 minutes, followed by resuspension in a 2 mL solution of methanol containing 20% FBS. A mixture of 4 mL collagen solution and 0.5 mL 10x Medium 199 was prepared, and the pH was adjusted by the addition of sterile ice-cold NaOH.

Subsequently, 2 mL of the collagen/Medium 199 solution was combined with the methanol solution containing the spheroids. For each well of a 24-well plate, 1 mL of the spheroid-collagen solution was added and allowed to incubate at a temperature of 37°C for a duration of 30 minutes to facilitate collagen polymerization. Spheroids were subjected to simulation by adding 200 μL of DMEM containing CuO NPs for a duration of 24 hours within a humidified incubator set at 37°C and 5% CO2. Subsequently, images were captured utilizing an Olympus microscope model IX81, and the quantification of sprouting numbers or vascular length was performed using ImageJ software.

Live/dead stain

The cytotoxicity of CuO NPs on HUVECs was assessed *in vitro* using the Live/Dead fixed cell staining method. HUVECs were seeded in 24-well plates at a density of 1 × 104 cells/well and cultured for 12 hours. Subsequently, CuO NPs were suspended in DMEM and co-incubated with the HUVECs for 24 hours. Following this, the cells were stained with calcein-AM to identify living cells and propidium iodide to identify dead or late apoptotic cells for a duration of 20 minutes. The cellular fluorescence was observed and recorded using an Olympus IX81 microscope.

Oxygen Induced Retinopathy

Oxygen-induced retinopathy (OIR) mouse model was established as we previously reported [20].

From postnatal day 7 (P7) to postnatal day 12 (P12), pups with their nursing mother were subjected to an oxygen concentration of 75%. Subsequently, they were exposed to room air for an additional 5 days. On postnatal day 13 (P13), the mice were randomly divided into two groups. One group received a single dose of CuO NPs (0.5μg) injected into the vitreous cavity, while the other group received a PBS injection (3μL). On postnatal day 17 (P17), the pups were euthanized, and their eyes were removed for subsequent immunofluorescence assays. Throughout the experiment, the oxygen levels were continuously monitored using an oxygen analyzer (XBS-03S, HangZhou Aipu Instrument Equipment, Hangzhou, China).

Retinal Vascular Development

To assess the effect of CuO NPs on the postnatal development of retinal angiogenesis, control pups and pups received intraperitoneal injection of 0.5 μg CuO NPs at P5. The pups were euthanized, and the eyes were harvested at P7. Whole-mount retinas were stained with IB4 and ERG as described in the *in vivo* endothelial cell proliferation sections. The ratio of the vascular area to the retinal area was used to quantify superficial vascular layer development.

In Vivo Endothelial Cell Proliferation

To investigate the *in vivo* proliferation of endothelial cells, we conducted a proliferation analysis using the Cell-LightTM EdU Apollo567 Kit. The staining procedure for EdU was carried out in accordance with the instructions provided by the manufacturer. P17 mice were administered with EdU (5 mg/kg)and euthanized after a 6-hour interval. The eyes were then removed and fixed in a 4% PFA solution for a

duration of 30 minutes at RT. Subsequently, the eyes were isolated under a microscope and subjected to blocking using a 1% BSA and 5% FBS buffer containing 0.5% Triton- X-100 for 30 minutes at RT. Following three washes in PBS, the retinas were subjected to overnight incubation at 4°C with FITC-conjugated Isolectin B4 and ERG primary antibodies(diluted at a ratio of 1:250 in a solution containing 1% BSA, 5% FBS, and 0.05% Triton-X-100 in PBS). Subsequently, the retinas underwent three additional washes with PBS. Next, the retinas were incubated with secondary antibodies for a duration of 2 hours at RT. Following another three washes with PBS, the retinas were incubated with EdU in accordance with the manufacturer's instructions. Finally, the retinas were mounted onto glass slides and sealed using a fluorescent mounting medium. A confocal microscope system (Leica TCS SP5-II) was used to capture the images, and Image J was used to quantify the avascular and neovascular areas. The Leica TCS SP5-II confocal microscope system was employed to acquire the images, while Image J software was utilized to quantify the avascular and neovascular areas.

RNA Sequencing

Cells in culture dishes were treated with CuO NPs for 48 h and total RNA prepared for RNA-seq analyses were extracted from cells using Trizol reagent as described by the manufacturer (Invitrogen). RNA sequencing and analysis were conducted at TIANGEN Biotech (Beijing) Co., Ltd. The pathway enrichment analysis was carried out using the KEGG database and GO database. A robust algorithm was employed to identify genes that were differentially expressed between two samples, following the principles described in "The significance of digital gene expression profiles". Multiple tests and analyses were performed, using a P value as the threshold for determining significance. Pathways with a P value < 0.05 were considered to have a significant enrichment of differentially expressed or modified genes.

Targeted metabolomic analysis

Cell supernatant was prepared for metabolomic analysis. Briefly, HUVECs treated with CuO NPs for 24 h were suspended in 400 μL of an extraction solution (methanol: acetonitrile: water (v/v/v, 4:4:1)). Afterwards, cells were submitted to Grinding treatment for 4 min, and were sonicated in an ultrasonic water bath for 20 min and incubated at -40°C for 1 h. Next, samples were centrifuged at 12000 g for 15 min at 4°C and the supernatant was spin dry under vacuum. The film was redissolved by the addition of pure water, followed by passing and collecting the supernatant. Subsequently, Shanghai iProteome Biotechnology Co., Ltd. conducted further analysis. HPIC-MS/MS analysis was carried out using a Thermo Scientific Dionex ICS-6000 HPIC high performance ion chromatograph with AS11-HC RFIC separation column. Mass spectrometry in multiple response monitoring (MRM) mode was performed using a 6500 QTrap + mass spectrometer. AB SCIEX Analyst Work Station Software, MultiQuant software, and Chromeleon7 were utilized for the acquisition of mass spectrum data and quantitative analysis of the target compounds.

Western Blotting

The extraction of total protein from cells or exosomes was performed using RIPA lysis buffer supplemented with 2% protease and protease inhibitor. The protein concentrations were determined using a standard trace bisphenolic acid assay (BCA, Beyotime, Shanghai, China) following the manufacturer's instructions. The samples were prepared in 5 × SDS-PAGE loading buffer and subjected to heating at 95°C for 10 minutes. Subsequently, the protein samples and protein markers were separated by 12.5% SDS-PAGE at 120 volts for 60 minutes and transferred to PVDF membranes at 100 V for 120 minutes. The membranes were blocked using a 5% nonfat dry milk solution in TBST (Tris-buffered saline with 0.1% Tween-20) for a duration of 2 hours at room temperature (RT). Subsequently, the membrane was briefly rinsed in TBST and incubated overnight at 4°C with primary antibodies diluted in a 5% BSA solution in TBST. The primary antibodies used in this study were summarized in Table S1. Following three washes in TBST, the membrane was incubated with a horseradish peroxidase-conjugated secondary IgG antibody (in a 5% non-fat dry milk solution) for 1.5 hours at RT. Following an additional three washes in TBST, chemiluminescence was observed using the ECL Western blotting detection reagent (Merck-Millipore, Darmstadt, Germany). The Gelview 6000Plus Image Capture System (Guangzhou Biolight Biotechnology Co., Ltd, Guangzhou, China) was employed to capture images, which were subsequently quantified using the ImageJ software.

Pyruvate Detection

The extracellular Pyruvate Levels were measured using the Pyruvate Assay Kit (Nanjing Jiancheng Bioengineering Institute, A081-1-1) according to the manufacturer’s instructions. In summary, a volume of 100 μL of cell lysate supernatant from HUVECs was added to a previously prepared 0.5 mL working solution and thoroughly mixed. The reaction was halted by the addition of 2.5 mL of a terminator solution after incubation at 37 ℃ for 10 minutes. Subsequently, 100 μL of the reaction mixtures were dispensed into a 96-well plate and the absorption peak at a wavelength of 505nm was quantified.

Blood routine examination and blood biochemistry analysis

In order to assess the blood compatibility of CuO NPs, an analysis of blood routine and biochemical indexes was conducted. C57BL/6 mice were utilized for the blood routine and biochemical evaluations. The mice were randomly allocated into twpo groups and received intravenous infusions of phosphate-buffered saline (PBS) and CuO NPs. Following a 14-day period, blood samples (100 μL) were obtained from the heart. The blood biochemical analysis was carried out using an LW C400 Mindray automatic biochemical analyzer (Shenzhen Lanyun Medical Equipment Co., Ltd., Shenzhen, China), while the routine examination analysis was performed using an automatic hematology analyzer (TEK8500 VET, Tecom Science, Jiangxi, China).

Statistical analysis

Statistical analysis was performed using ImageJ software (ImageJ software, 1.52a National Institutes of Health, Bethesda, MD, USA) and GraphPad Prism (GraphPad software 9.0, GraphPad, Bethesda, MD, USA) and. The measurement data of the two groups were subjected to analysis using an unpaired Student's t-

test, while the comparison among multiple groups was conducted through one-way analysis of variance (ANOVA). Each experiment was replicated three times, and statistical significance was determined at a threshold of $P < 0.05$ (* $P < 0.05$; ** $P < 0.01$; *** $P < 0.001$; **** $P < 0.0001$).

3 Results

Characterization and biocompatibility of CuO NPs

The transmission electron microscopy (TEM) analysis revealed the microscopic morphology of CuO NPs, which exhibited a uniform and sphericalshape. The size distribution of the nanoparticles ranged from 11 to 27nm, with a mean diameter of 18.9nm (Fig. 2A,B). Furthermore, the size and zeta potential of nanoparticles are crucial physicochemical properties that serve as reliable indicators for studying their characteristics and play a significant role in cellular endocytosis. The zeta potential spectrum of CuO NPs, depicted in Fig. 2C, exhibited a value of -24.35 ± 1.32mV. These findings collectively demonstrate the well stability of CuO NPs.

HUVECs were subjected to incubation with varying concentrations of CuO NPs (3, 6, 12, 24, 48, 96, and 192 μg/ml) for a duration of 24 hours, and the cell viability was measured using the Cell Counting Kit-8 (CCK8) assay. As shown in Fig. 2D, the cell viability of HUVECs treated with 3 and 6 μg/ml CuO NPs did not exhibit a significant difference compared to those treated with 0 μg/ml CuO NPs. However, exposure of HUVECs to concentrations of CuO NPs at 12, 24, 48, 96, and 192 μg/ml resulted in a dose-dependent inhibition of HUVEC viability (Fig. 2D). The concentrations of CuO NPs at 12 and 24μg/ml were selected as appropriate concentration for subsequent experiments. In order to further evaluate the biocompatibility of CuO NPs, a cell live/dead assay was conducted. HUVECs were exposed to 24 μg/ml CuO NPs for a duration of 24 hours, followed by staining with Calcein-AM (CAM) and Propidium Iodide (PI). The observed percentages of PI-positive cells in HUVECs treated with 0 and 24μg/ml CuO NPs were 0.22% and 0.24% respectively, indicating that the presence of 24 μg/ml CuO NPs did not result in significant cellular toxicity (Fig. 2E,F). Furthermore, the *in vivo* systemic toxicity of CuO NPs was assessed through histological and hematology analysis. The results indicated that the morphology of the major internal organs, including the heart, liver, spleen, lung, and kidney, stained with Hematoxylin and eosin (H & E), did not exhibit any apparent abnormalities (Additional file : Fig. S1). Meanwhile, the findings from the hematology analysis revealed that CuO NPs did not have any impact on the blood routine and blood biochemical indicators (Additional file : Fig. S3 and S4).

CuO NPs inhibit angiogenesis in vitro

Cell proliferation, migration, tube formation and sprouting are crucial physiological process of vascular endothelial cells that contribute to angiogenesis. In this study, we conducted an analysis to investigate the impact of CuO NPs on the proliferation activity of endothelial cells using the 5-ethynyl-2-deoxyuridine (EdU) assay. Our findings revealed that treatment with CuO NPs resulted in a significant reduction in the proportion of EdU positive cells, in a dose-dependent manner, when compared to the control group (Fig. 3A,B). Cell tube formation is one of the key processes for angiogenesis. The findings of this study

demonstrate that CuO NPs at concentrations of 12 and 24 μg/ml hindered the ability of vascular endothelial cells to form tubes (Fig. 3C,D). Additionally, we employed wound healing assays to assess the migration ability of HUVECs after treated with CuO NPs. Our results demonstrated that CuO NPs hindered cell migration in a dose-dependent manner (Fig. 3E,F). Sprouting, a fundamental process in vascular growth and angiogenesis, was also significantly suppressed by CuO NPs. This suppression was evident in the reduced numbers of sprouts, shorter sprout length, and decreased cumulative sprout length (Fig. 3G-J). These results indicate that CuO NPs possess the capacity to inhibit neovascularization *in vitro* in a dose-dependent manner.

CuO NPs suppress mouse retinal vascular development

In order to evaluate the *in vivo* anti-angiogenic effect of CuO NPs, we employed the widely accepted mouse retinal angiogenesis model. The results suggested that P7 pups received intraperitoneal injections of CuO NPs, displayed a delayed expansion of the vascular plexus towards the periphery. This characteristic was particularly prominent at the site of angiogenesis, whereas the pre-existing central portion of the retinal vasculature showed comparatively lesser impact (Fig. 4A-B). Furthermore, the retinal vascular density and the number of filopodia in the sprouting region of mice treated with CuO NPs exhibited a significant reduction in comparison to the control group. The findings indicate a significant inhibition of endothelial cell proliferation by CuO NPs (Fig. 4C-E). Notably, at postnatal seven days (P7) and P17, CuO NPs did not elicit any discernible retinal toxicity, as evidenced by the absence of alterations in retinal morphology (Additional file : Fig. S2).

CuO NPs suppresses pathological retinal angiogenesis in vivo

The oxygen-induced retinopathy (OIR) model is widely used for the study of neovascular mechanisms. In this study, mice were subjected to a hypoxic environment for 5 days starting on P7, followed by exposure to a normal oxygen environment on P12. This experimental protocol resulted in the development of relatively low oxygen conditions and the formation of pathological neovascularization and non-perfusion zones in the retinas of the mice (Fig. 5A). Following this, the retinas of the mice were surgically removed on P17 and subsequently subjected to immunofluorescence staining. The findings revealed that, in comparison to the control group, the administration of CuO NPs resulted in a decrease in retinal neovascularization and a reduction of non-perfusion areas within the mouse retina (Fig. 5A-C). Subsequently, the retina was subjected to staining with EdU in order to examine the impact of CuO NPs on the proliferative behavior of vascular endothelial cells. The results revealed a notable reduction in the proliferative activity of retinal endothelial cells among mice treated with CuO NPs, as compared to the control group (Fig. 5D,E).

Targeted metabolomics suggests disrupted TCA cycle after CuO NPs treatment

To investigate the inhibitory mechanism of CuO NPs on HUVECs proliferation, a targeted metabolomic approach was employed. The analysis revealed alterations in 50 metabolites, with 36 metabolites showing up-regulation and 14 metabolites displaying down-regulation (Fig. 6A). Additionally, it was

observed that the levels of pyruvate and alpha-ketoglutaric acid were elevated, while succinic acid levels were reduced (Fig. 6A-D). Subsequent examination of intracellular pyruvate levels confirmed the accumulation of pyruvate in endothelial cells treated with CuO NPs (Fig. 6E). These changes were related to the inhibition of the TCA cycle. Further enrichment analysis of the Kyoto Encyclopedia of Genes and Genomes (KEGG) signaling pathway revealed that differentially expressed metabolites were enriched in the TCA cycle (Fig. 6F-I). Recent studies have indicated that the disturbance of the TCA cycle is a characteristic feature of Cuproptosis [16]. This process involves in the direct binding of copper ions to lipoylated components of the TCA cycle, in which lead to the aggregation of fatty acylated proteins and the loss of iron-sulfur proteins. Consequently, we propose the hypothesis that CuO NPs enhance the copper burden of HUVECs and hinder the development of HUVECs by inducing cuproptosis.

RNA-seq data indicates disrupted TCA cycle and induced cuproptosis by CuO NPs

To investigate the induction of cuproptosis in endothelial cells by CuO NPs, an RNA-seq analysis was conducted. The results revealed alterations in a total of 6030 genes, with 2933 genes showing up-regulation and 3097 genes showing down-regulation (Fig. 7A). The KEGG and GO pathway analysis demonstrated that the down-regulated genes were significantly enriched in the TCA cycle (Fig. 7B-C), which aligns with the findings of the metabolomic analysis (Fig. 5F-I). Furthermore, among the 296 downregulated genes, three cuproptosis-related genes (DLAT, SDHB, and FDX1) were included (Fig. 7D). DLAT, a subunit of the pyruvate dehydrogenase complex, plays a crucial role in regulating the entry of carbon into the TCA cycle. The reductase FDX1 is responsible for reducing Cu^{2+} to the more toxic Cu^{+}, which subsequently promotes the oligomerization of DLAT and increases the insoluble form of DLAT [16, 21]. This process ultimately results in proteotoxic stress and cell death[16, 22]. Additionally, the down-regulation of SDHB, an iron-sulfur (Fe-S) cluster protein, is observed due to the interference of Cu^{+} with Fe-S cluster proteins, leading to the loss of these important proteins[16, 18]. In order to provide additional evidence for our hypothesis, we conducted a western blot analysis to evaluate the protein levels related to cuproptosis in endothelial cells treated with CuO NPs. The outcomes of this analysis were in line with the findings from the RNA-seq analysis, indicating a notable decrease in the expression of DLAT, SDHB, and FDX1 (Fig. 7E-F). In summary, the findings of this study have the potential to support the hypothesis that CuO nanoparticles play a role in mitochondrial proteotoxicity and ultimately lead to the induction of cuproptosis.

4 Discussion

Angiogenesis is a complex physiological phenomenon involving the development of new capillary blood vessels from pre-existing vascular networks, while the pathological angiogenesis in the retina is characterized by the abnormal and swift proliferation of endothelial cells within blood vessels.[23]. This pathological progression would lead to complications such as hemorrhaging, vascular permeability, and tissue harm. It represents a prevalent pathological characteristic observed in diverse fundus diseases with great threaten to vision outcome [24]. The murine OIR model and retinal vascular development model have been widely used in the investigation of pathological retinal angiogenesis. In this study, the

utilization of these two models was employed to examine the potential anti-angiogenic effects of CuO NPs [25, 26].

In recent years, there has been a large number of investigations regarding the application of copper-based nanoparticles in the field of tumor therapy [27–29]. Yao Lu's research indicate that a nanoplatform based on CuO NPs can effectively alleviate osteoarthritis by impeding the PI3K/AKT/mTOR pathway [30]. It is noteworthy that both uncontrolled cell proliferation and persistent inflammatory reactions in tumorigenesis are shared characteristics in pathological angiogenesis of the retina. Hence, we hypothesized that CuO NPs possessed anti-angiogenic properties within the context of pathological angiogenesis in the retina. In this study, we examined the anti-angiogenic properties of CuO NPs both *in vitro* and *in vivo*. Our findings indicated that CuO NPs effectively suppressed the proliferation, migration, tube formation, and sprouting of endothelial cells *in vitro* dose dependently. The results obtained from *in vivo* experiments indicated that CuO NPs possess significant anti-angiogenic properties. Treatment with CuO NPs resulted in a reduction in both neovascularization and avascular area in the OIR model, indicating an improvement of pathological retinopathy [31]. Additionally, the development of retinal vasculature was inhibited following treatment with CuO NPs. Besides, CuO NPs did not cause toxicity in ECs and in the major organs of mice. These findings suggest that CuO NPs have the potential to be utilized as nanomedicines for the treatment of pathological angiogenesis.

Cuproptosis is a novel form of copper-dependent cell death that is distinct from known regulated cell death pathways including apoptosis, necroptosis, and ferroptosis. Tsvetkov et al. provided evidence that Elesclomol, a copper ionophore, is capable of transporting copper ions to the mitochondria of cells and inducing cuproptosis [16]. The excess copper irectly binds to lipoacylated components of the TCA cycle, resulting in the aggregation of lipoacylated proteins and loss of iron–sulfur cluster proteins. This process induces proteotoxic stress and ultimately leads to cell death [16, 32].. Pathological neovascularization refers to the uncontrolled and rapid proliferation of endothelial cells. During the progression, tricarboxylic acid (TCA) cycle in mitochondria plays a crucial role, which is responsible for generating energy [33]. Previous researchs suggest that copper ions directly interact with lipoylated components of the TCA cycle during cuproptosis, leading to the disruption of this metabolic pathway [16, 18, 34]. Through our metabolomics analysis, we observed that exposure to CuO NPs results in increased levels of pyruvate and alpha-ketoglutaric acid, and accompanied by a decrease in succinic acid levels. These data showed evidence for the disruption of the TCA cycle induced by CuO NPs[35, 36]. Furthermore, Tsvetkov et al [16] have identified a set of crucial genes or proteins implicated in the cuproptosis mechanism, which is strongly linked to copper imbalance. In our present study, we performed RNA-sequence and western blot analyses, unveiling a reduction in both mRNA and protein levels of cuproptosis-related proteins (DLAT, FDX1, and SDHB) after CuO NPs treatment. Additionally, the KEGG and GO pathway analysis exhibited a significant enrichment of down-regulated genes in the TCA cycle. These findings indicated that CuO NPs play a role in mitochondrial proteotoxicity, leading to cell death via the mechanism of cuproptosis.

5 Conclusion

In conclusion, this study conducted an assessment of the anti-angiogenic properties of CuO NPs both *in vitro* and *in vivo*. The findings demonstrated that CuO NPs exhibited significant inhibition of endothelial cell proliferation, migration, tube formation, and sprouting. Furthermore, CuO NPs effectively suppressed oxygen-induced retinopathy and retinal vascular development in mice. Through a combined analysis of metabolomics and RNA sequencing, it was revealed that CuO NPs disrupted the TCA cycle pathway, ultimately leading to cuproptosis. These results indicate that CuO NPs possess considerable therapeutic potential for the treatment of pathological angiogenesis, offering a promising alternative approach for angiogenesis therapy.

Declarations

Supplementary information

Supplementary information is available from the author.

Acknowledgments

We are grateful to Youheng Wei (State Key Laboratory of Genetic Engineering, Institute of Genetics, Fudan University, Shanghai, China) for providing technical assistance. Illustrations were created with BioRender.com. Funding: This work was supported by funding from National Natural Science Foundation of China (grant 82271106 and 82171081), Shanghai Pujiang Program (grant 21PD068), Shanghai Science and Technology committee (grant 22ZR1478200), Shanghai Chen Guang project (grant 18CG40).

Competing interests

All authors declare they have no competing interests.

Availability of data and materials

All data are available in the main text or the supplementary materials.

Author contributions

Conceptualization: H. S and W. S. Methodology: H. Z, C. C, Q. L and M. W. Investigation: H. Z, C.C, Q. L, Z. N & Y. L. Visualization: H. Z and C.C. Funding and Supervision: H. S and W. S. Writing—original draft: H. Z and C. C. Writing—review & editing: H. S, H. Z and C. C.

References

1. Antonetti DA, Silva PS, Stitt AW: Current understanding of the molecular and cellular pathology of diabetic retinopathy. Nat Rev Endocrinol 2021, 17(4):195-206.

2. Augustin HG, Koh GY: Organotypic vasculature: From descriptive heterogeneity to functional pathophysiology. Science 2017, 357(6353).
3. Antoszyk AN, Glassman AR, Beaulieu WT, Jampol LM, Jhaveri CD, Punjabi OS, Salehi-Had H, Wells JA, 3rd, Maguire MG, Stockdale CR *et al*: Effect of Intravitreous Aflibercept vs Vitrectomy With Panretinal Photocoagulation on Visual Acuity in Patients With Vitreous Hemorrhage From Proliferative Diabetic Retinopathy: A Randomized Clinical Trial. Jama 2020, 324(23):2383-2395.
4. Tian Y, Zhang F, Qiu Y, Wang S, Li F, Zhao J, Pan C, Tao Y, Yu D, Wei W: Reduction of choroidal neovascularization via cleavable VEGF antibodies conjugated to exosomes derived from regulatory T cells. Nat Biomed Eng 2021, 5(9):968-982.
5. Mettu PS, Allingham MJ, Cousins SW: Incomplete response to Anti-VEGF therapy in neovascular AMD: Exploring disease mechanisms and therapeutic opportunities. Prog Retin Eye Res 2021, 82:100906.
6. Usui-Ouchi A, Friedlander M: Anti-VEGF therapy: higher potency and long-lasting antagonism are not necessarily better. J Clin Invest 2019, 129(8):3032-3034.
7. Gawande MB, Goswami A, Felpin FX, Asefa T, Huang X, Silva R, Zou X, Zboril R, Varma RS: Cu and Cu-Based Nanoparticles: Synthesis and Applications in Catalysis. Chem Rev 2016, 116(6):3722-3811.
8. Mani VM, Kalaivani S, Sabarathinam S, Vasuki M, Soundari A, Ayyappa Das MP, Elfasakhany A, Pugazhendhi A: Copper oxide nanoparticles synthesized from an endophytic fungus Aspergillus terreus: Bioactivity and anti-cancer evaluations. Environ Res 2021, 201:111502.
9. Abbasi A, Ghorban K, Nojoomi F, Dadmanesh M: Smaller Copper Oxide Nanoparticles have More Biological Effects Versus Breast Cancer and Nosocomial Infections Bacteria. Asian Pac J Cancer Prev 2021, 22(3):893-902.
10. Sathiyavimal S, Vasantharaj S, Kaliannan T, Garalleh HA, Garaleh M, Brindhadevi K, Chi NTL, Sharma A, Pugazhendhi A: Bio-functionalized copper oxide/chitosan nanocomposite using Sida cordifolia and their efficient properties of antibacterial, anticancer activity against on breast and lung cancer cell lines. Environ Res 2023, 218:114986.
11. Pillai RR, Sreelekshmi PB, Meera AP: Enhanced biological performance of green sythesized copper oxide nanoparticles using Pimenta dioica leaf extract. Materials Today: Proceedings 2022, 50:163-172.
12. Guan G, Zhang L, Zhu J, Wu H, Li W, Sun Q: Antibacterial properties and mechanism of biopolymer-based films functionalized by CuO/ZnO nanoparticles against Escherichia coli and Staphylococcus aureus. J Hazard Mater 2021, 402:123542.
13. Bezza FA, Tichapondwa SM, Chirwa EMN: Fabrication of monodispersed copper oxide nanoparticles with potential application as antimicrobial agents. Sci Rep 2020, 10(1):16680.
14. Verma N, Kumar N: Synthesis and biomedical applications of copper oxide nanoparticles: an expanding horizon. ACS biomaterials science & engineering 2019, 5(3):1170-1188.

15. Verma N, Kumar N: Synthesis and Biomedical Applications of Copper Oxide Nanoparticles: An Expanding Horizon. ACS Biomater Sci Eng 2019, 5(3):1170-1188.
16. Tsvetkov P, Coy S, Petrova B, Dreishpoon M, Verma A, Abdusamad M, Rossen J, Joesch-Cohen L, Humeidi R, Spangler RD *et al*: Copper induces cell death by targeting lipoylated TCA cycle proteins. Science 2022, 375(6586):1254-1261.
17. Guo B, Yang F, Zhang L, Zhao Q, Wang W, Yin L, Chen D, Wang M, Han S, Xiao H *et al*: Cuproptosis Induced by ROS Responsive Nanoparticles with Elesclomol and Copper Combined with αPD-L1 for Enhanced Cancer Immunotherapy. Adv Mater 2023, 35(22):e2212267.
18. Ning S, Lyu M, Zhu D, Lam JWY, Huang Q, Zhang T, Tang BZ: Type-I AIE Photosensitizer Loaded Biomimetic System Boosting Cuproptosis to Inhibit Breast Cancer Metastasis and Rechallenge. ACS Nano 2023, 17(11):10206-10217.
19. Liu WQ, Lin WR, Yan L, Xu WH, Yang J: Copper homeostasis and cuproptosis in cancer immunity and therapy. Immunol Rev 2023.
20. Gui X, Zhang H, Zhang R, Li Q, Zhu W, Nie Z, Zhao J, Cui X, Hao W, Wen X *et al*: Exosomes incorporated with black phosphorus quantum dots attenuate retinal angiogenesis via disrupting glucose metabolism. Mater Today Bio 2023, 19:100602.
21. Lee SY, Seo JH, Kim S, Hwang C, Jeong DI, Park J, Yang M, Huh JW, Cho HJ: Cuproptosis-Inducible Chemotherapeutic/Cascade Catalytic Reactor System for Combating with Breast Cancer. Small 2023, 19(35):e2301402.
22. Ding H, Ren F, Liu P, Feng Y, Ma X, Shen Z, Shi Q, Xu M, Li W, Chen H: Cu2+-Anchored Carbon Nano-Photocatalysts for Visible Water Splitting to Boost Hydrogen Cuproptosis. Angew Chem Int Ed Engl 2023:e202311549.
23. Carmeliet P: Mechanisms of angiogenesis and arteriogenesis. Nat Med 2000, 6(4):389-395.
24. Uemura A, Fruttiger M, D'Amore PA, De Falco S, Joussen AM, Sennlaub F, Brunck LR, Johnson KT, Lambrou GN, Rittenhouse KD *et al*: VEGFR1 signaling in retinal angiogenesis and microinflammation. Prog Retin Eye Res 2021, 84:100954.
25. Vähätupa M, Järvinen TAH, Uusitalo-Järvinen H: Exploration of Oxygen-Induced Retinopathy Model to Discover New Therapeutic Drug Targets in Retinopathies. Front Pharmacol 2020, 11:873.
26. Falero-Perez J, Sorenson CM, Sheibani N: Cyp1b1-deficient retinal astrocytes are more proliferative and migratory and are protected from oxidative stress and inflammation. Am J Physiol Cell Physiol 2019, 316(6):C767-c781.
27. Chen T, Zeng W, Liu Y, Yu M, Huang C, Shi Z, Lin C, Tang J, Mei L, Wu M: Cu-Doped Polypyrrole with Multi-Catalytic Activities for Sono-Enhanced Nanocatalytic Tumor Therapy. Small 2022, 18(29):e2202964.
28. Meng X, Zhou K, Qian Y, Liu H, Wang X, Lin Y, Shi X, Tian Y, Lu Y, Chen Q *et al*: Hollow Cuprous Oxide@Nitrogen-Doped Carbon Nanocapsules for Cascade Chemodynamic Therapy. Small 2022, 18(15):e2107422.

29. Wu H, Chen F, You C, Zhang Y, Sun B, Zhu Q: Smart Porous Core-Shell Cuprous Oxide Nanocatalyst with High Biocompatibility for Acid-Triggered Chemo/Chemodynamic Synergistic Therapy. Small 2020, 16(45):e2001805.
30. Lu Y, Chen J, Li L, Cao Y, Zhao Y, Nie X, Ding C: Hierarchical functional nanoparticles boost osteoarthritis therapy by utilizing joint-resident mesenchymal stem cells. J Nanobiotechnology 2022, 20(1):89.
31. Kim CB, D'Amore PA, Connor KM: Revisiting the mouse model of oxygen-induced retinopathy. Eye Brain 2016, 8:67-79.
32. Tsvetkov P, Detappe A, Cai K, Keys HR, Brune Z, Ying W, Thiru P, Reidy M, Kugener G, Rossen J *et al*: Mitochondrial metabolism promotes adaptation to proteotoxic stress. Nat Chem Biol 2019, 15(7):681-689.
33. Lunt SY, Vander Heiden MG: Aerobic glycolysis: meeting the metabolic requirements of cell proliferation. Annu Rev Cell Dev Biol 2011, 27:441-464.
34. Lee SY, Seo JH, Kim S, Hwang C, Jeong DI, Park J, Yang M, Huh JW, Cho HJ: Cuproptosis-Inducible Chemotherapeutic/Cascade Catalytic Reactor System for Combating with Breast Cancer. Small 2023:e2301402.
35. Besse A, Wu P, Bruni F, Donti T, Graham BH, Craigen WJ, McFarland R, Moretti P, Lalani S, Scott KL *et al*: The GABA transaminase, ABAT, is essential for mitochondrial nucleoside metabolism. Cell Metab 2015, 21(3):417-427.
36. Hang J, Chen Y, Liu L, Chen L, Fang J, Wang F, Wang M: Antitumor effect and metabonomics of niclosamide micelles. J Cell Mol Med 2022, 26(18):4814-4824.

Figures

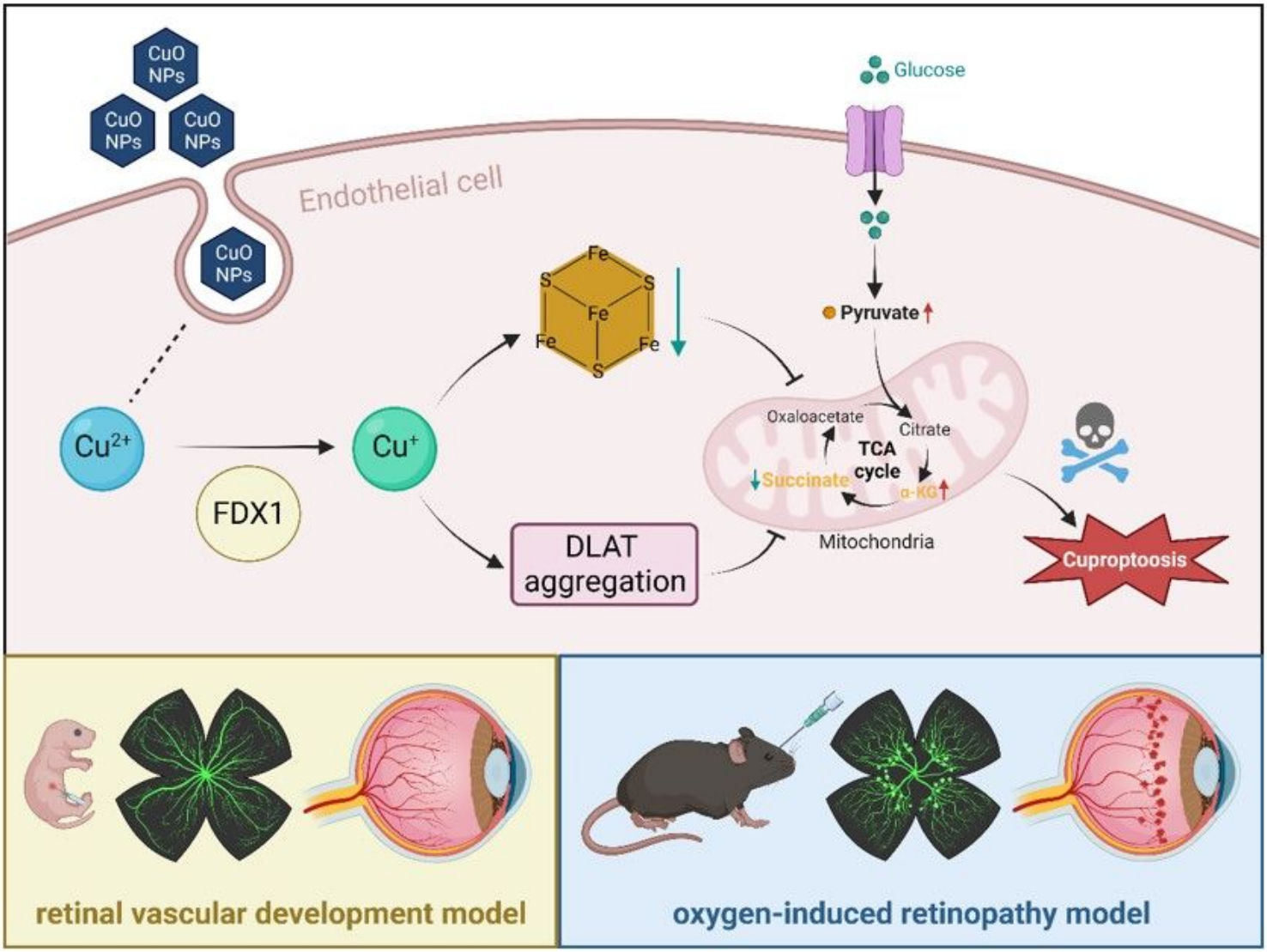

Figure 1

Schematic illustration of CuO NPs promoting cuproptosis and inhibiting retinal angiogenesis.

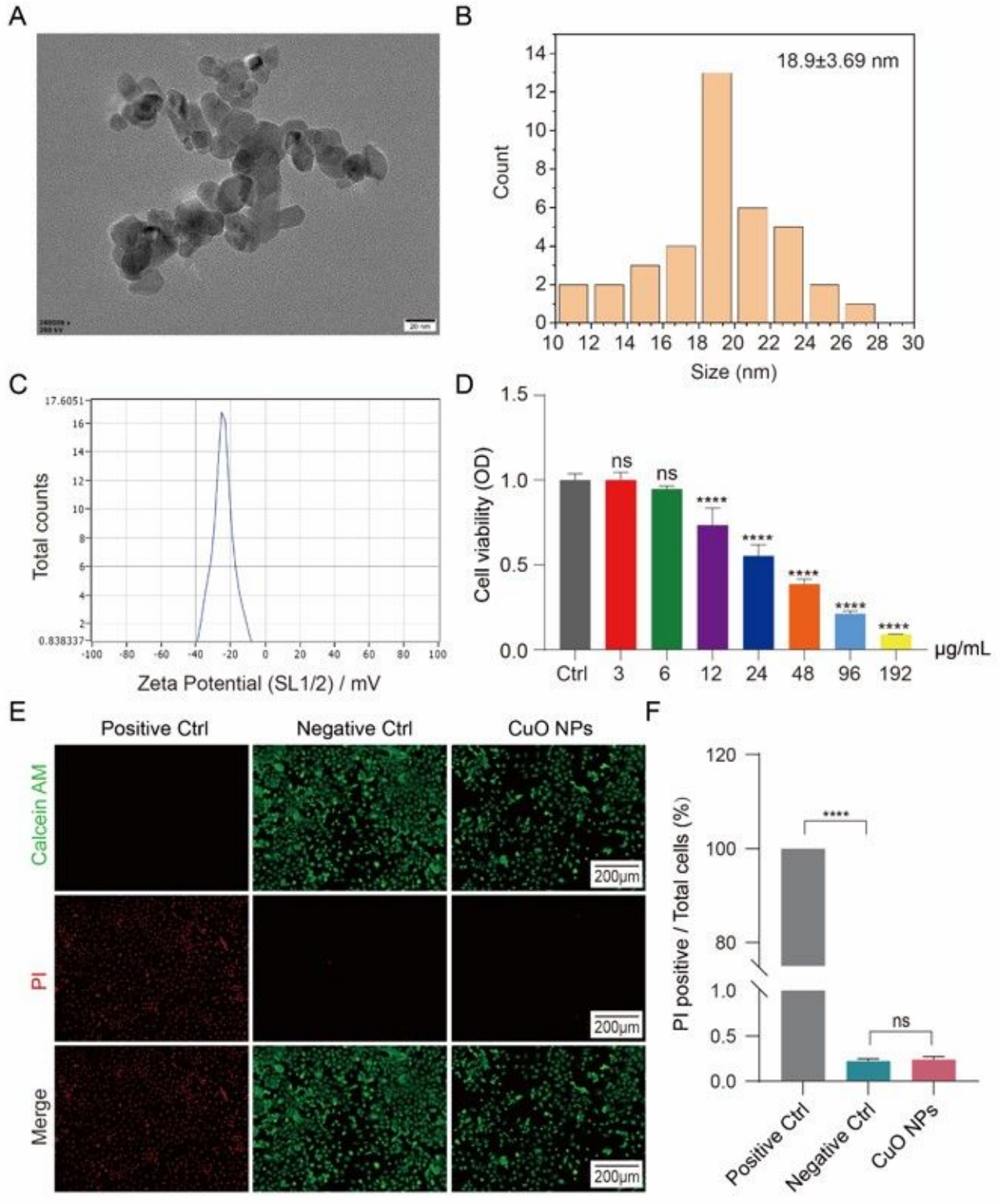

Figure 2

Characterization of the CuO NPs. (A) Representative TEM image. Scale bar: 20nm. (B) Size distribution of CuO NPs. (C) Zeta potential of CuO NPs. (D) CCK-8 assay showing cell viability. Data was presented as means ± Standard Deviation (SD), n=3, one-way ANOVA; ****P<0.0001. (E) Representative fluorescence images of live/dead assay of HUVECs treated with 24 μg/ml CuO NPs. Live cells (Green), Dead cells

(Red). Scale bar: 200 μm. (F) Statistical result of live/dead assay. Data was presented as means ± SD, n=3, one-way ANOVA; ****P <0.0001.

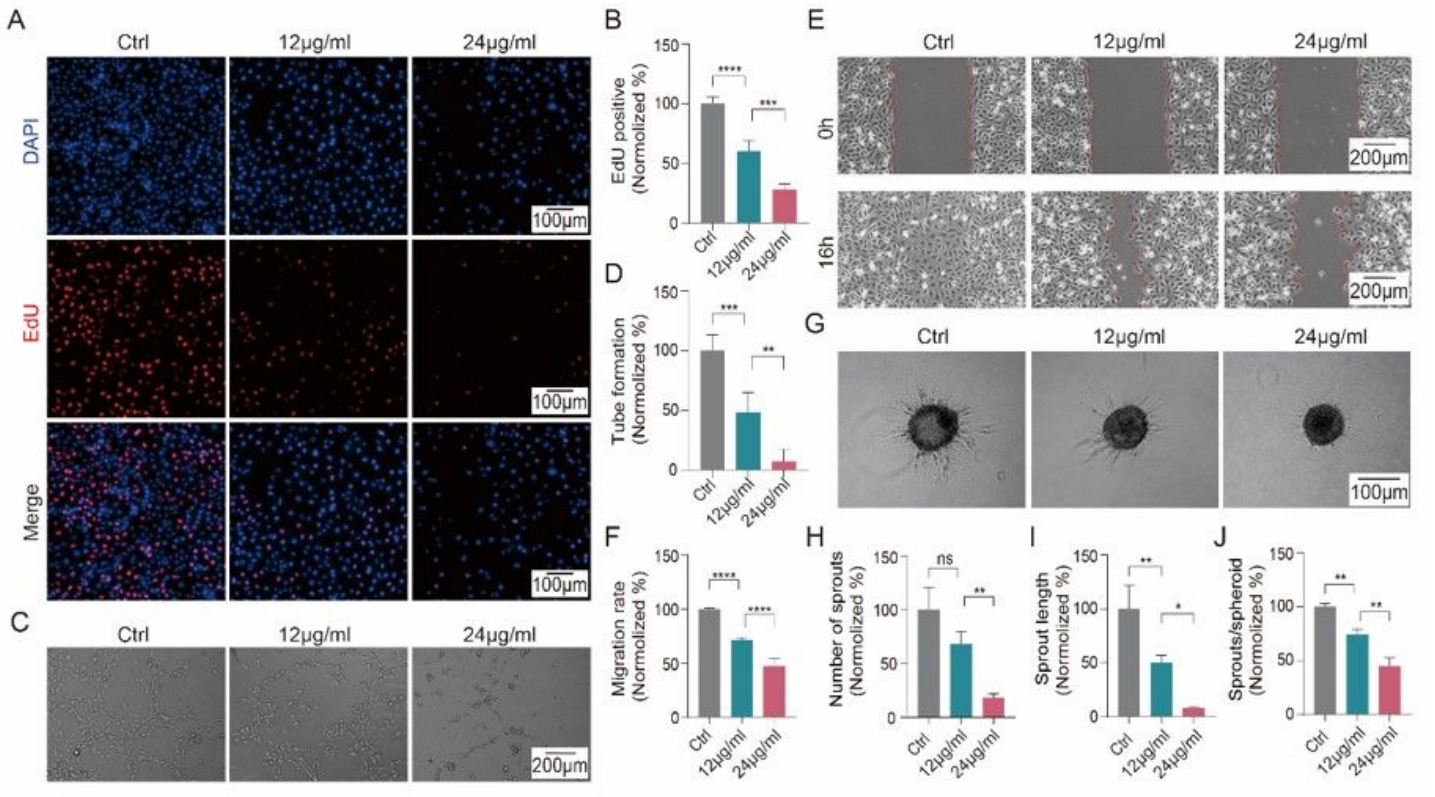

Figure 3

CuO NPs inhibits angiogenesis *in vitro*. (A) Representative images of HUVECs in EdU incorporation assay after exposure to CuO NPs. EdU positive cells (Red), Hochest positive cells (Blue). Scale bar: 100 μm. (B) Statistical result of cell proliferation. Data was presented as means ± SD, n=3, one-way ANOVA; ***P <0.001, ****P <0.0001. (C) Representative images of the HUVECs for tube formation assay after treatment with CuO NPs for 24h. Scale bar: 200 μm. (D) Statistical result of tube formation. Data was presented as means ± SD, n=3, one-way ANOVA; **P <0.01, ***P <0.001. (E) Representative images of the HUVECs for migration after exposure to CuO NPs for 24h. Scale bar: 200 μm. (F) Statistical result of migration. Data was presented as means ± SD, n=3, one-way ANOVA; ****P <0.0001. (G) Representative images of HUVECs for sprouting assay treated with CuO NPs for 24 h. Scale bar: 100 μm. (H-J) Statistical result of sprouting. Data was presented as means ± SD, n=3, one-way ANOVA; *P <0.05, **P <0.001.

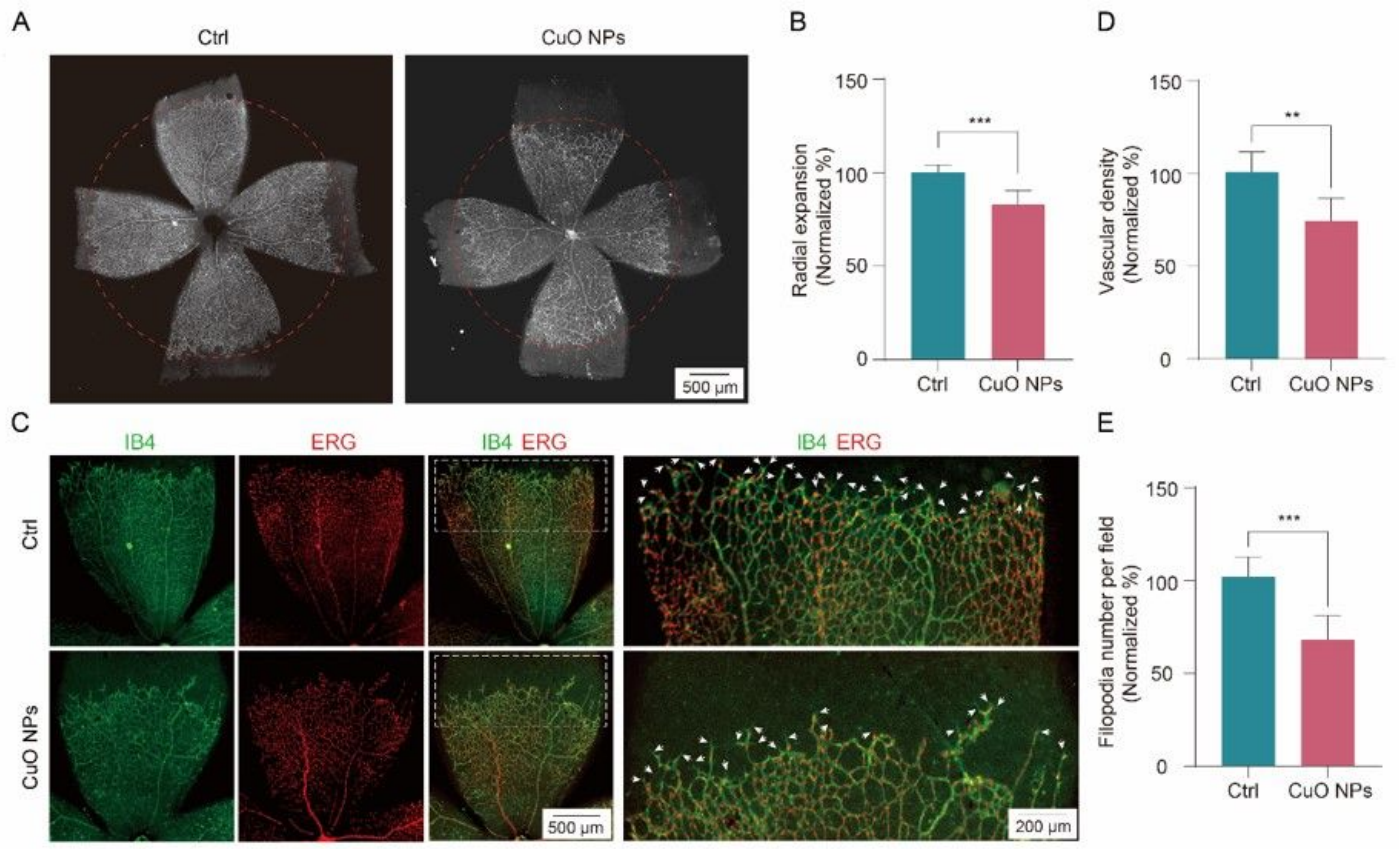

Figure 4

CuO NPs suppress retinal vascular development. (A) Representative images of retinas treated with CuO NPs at P2-P4 and harvested at P7. IB4 positive (White). Scale bar: 500μm. (B) Statistical result of retinal vascular development. Data was presented as means ± SD, n=8, two-tailed t test; ***P<0.001. (C) Immunofluorescence staining of ERG (red) and IB4 (green) in P7 mouse retinas. The white arrows indicate filopodia staining. Scale bar: 500μm (Left), 200μm (Right).(D-E) Statistical results of vascular density and filopodia. Data was presented as means ± SD, n=8, two-tailed t test; **P<0.01, ***P<0.001.

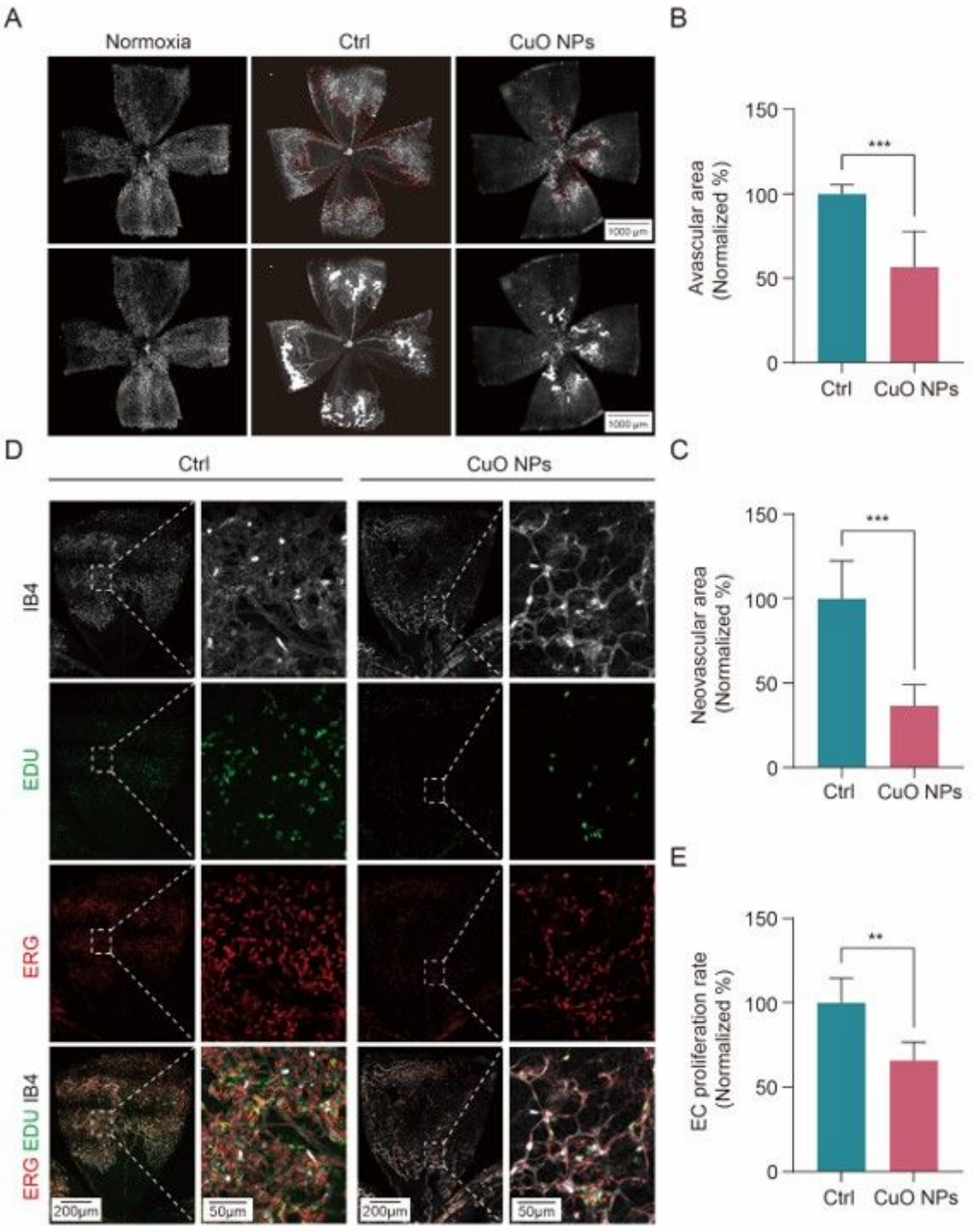

Figure 5

CuO NPs suppresses pathological retinal angiogenesis *in vivo*. (A) Representative images of OIR P17 mouse retinas administrated with CuO NPs. The red dotted line indicates avascular area in the central retina and the white area represents the neovascular tufts in retina. Scale bar: 1000μm. (B-C) Quantification of avascular area and neovascular tufts of retina. (D) Representative confocal immunofluorescence images of EdU (green), ERG (red) and IB4 (white) in P17 mouse retinas. Scale bar:

200μm, 50μm. (E) Statistical result of proliferating HUVECs. Data was presented as means ± SD, n=8, two tailed t test; **P <0.01, ***P <0.001.

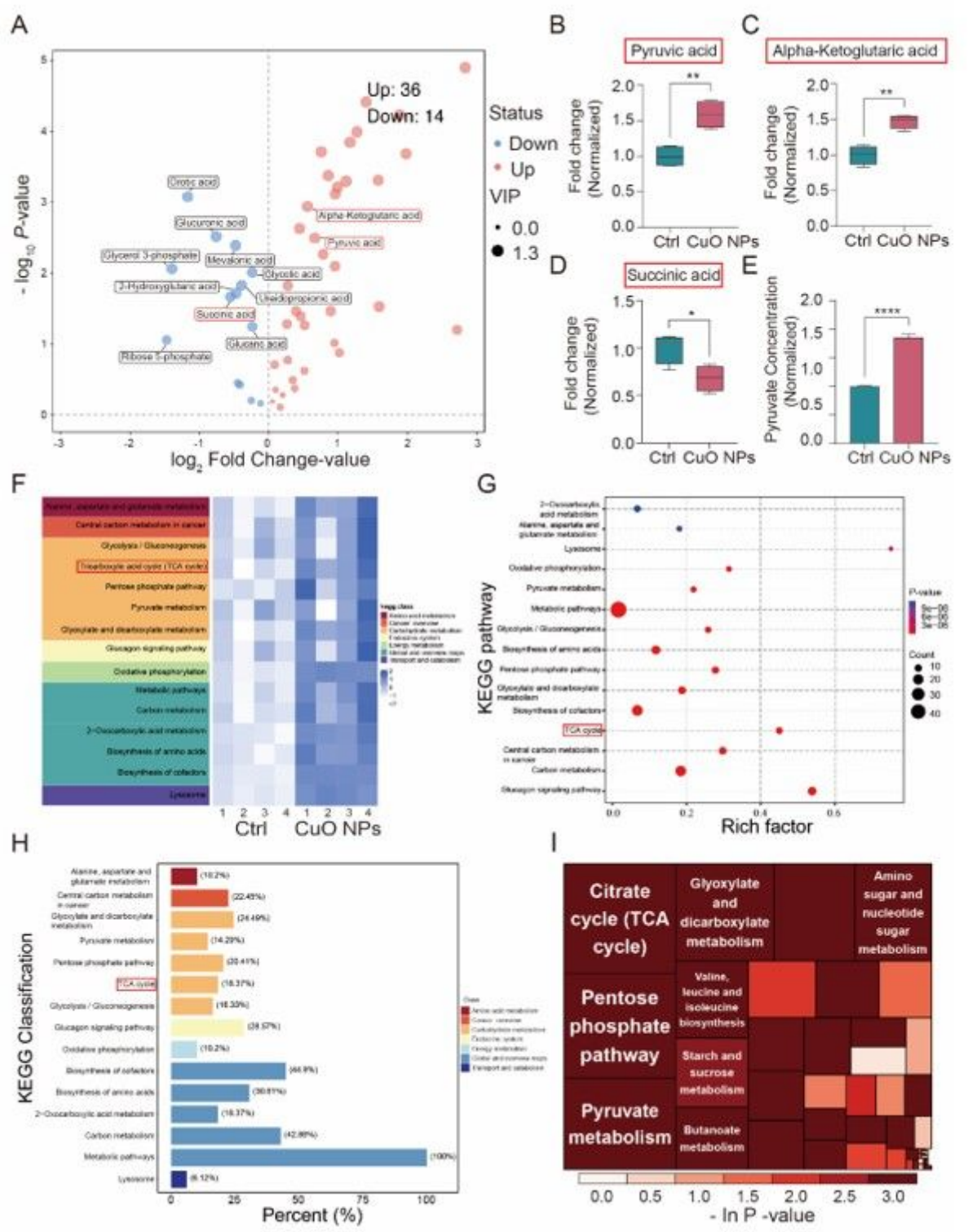

Figure 6

Targeted metabolomics showed inhibition of the TCA cycle. (A) Volcano plot of Log2 (fold-changed) versus -$\log_{10}$(P-value) of all annotated metabolites. (B-D) Pyruvic acid, alpha-ketoglutaric acid and succinic acid level of targeted metabolomics. (E) *In vitro* validation of Pyruvic acid accumulation in

HUVECs following treatment with CuO NPs. Data was presented as means ± SD, n=3, two tailed t test; ****P <0.0001. (F-I) The relative content of differential metabolites from the heat map (F), KEGG Enrichment pathyway (G), KEGG Classification(H) and KEGG heatmap (I).

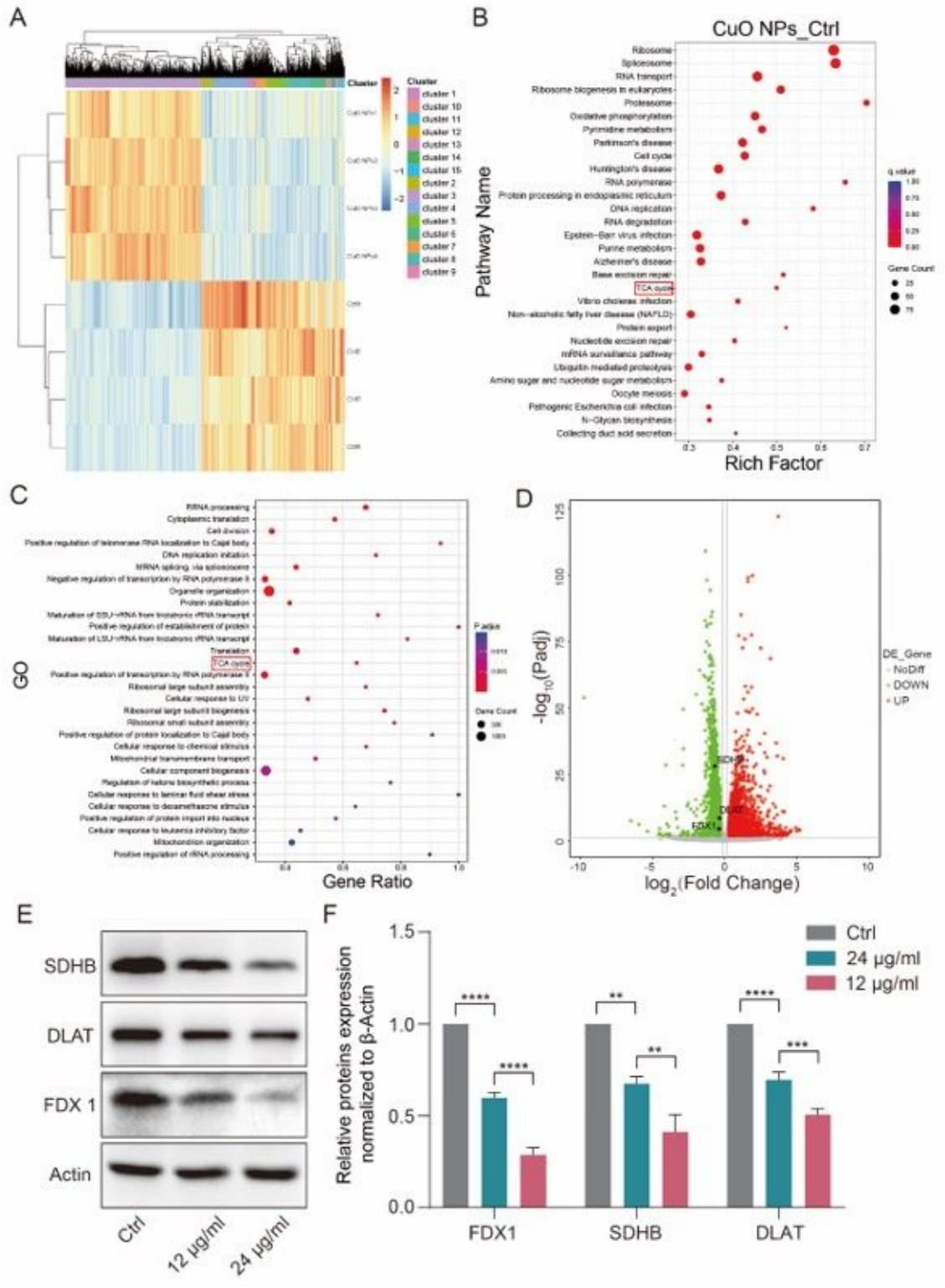

Figure 7

CuO NPs disrupt TCA cycle and induce cupropotosis. (A) The gene expression heatmap. Red for up-regulation; Blue for down-regulation. (B) Down-regulated genes enriched in KEGG pathways. (C) Down-regulated genes enriched in GO pathways. (D) Volcano plot of Log1.2 fold-changed genes for CuO NPs treatment. (E) The protein levels of SDHB, DLAT and FDX1 in CuO NPs treated HUVECs. (F) Statistical result of the protein levels. Data was presented as means ± SD, n=3, one-way ANOVA; **P <0.01; ***P <0.001; ****P <0.0001.

Supplementary Files

This is a list of supplementary files associated with this preprint. Click to download.

- SupportingInformation.docx